ASTROBIOLOGY
Volume 23, Number 4, 2023
Mary Ann Liebert, Inc.
DOI: 10.1089/ast.2022.0056

Research Article

Open camera or QR reader and scan code to access this article and other resources online.

Novel Chimeric Amino Acid-Fatty Alcohol Ester Amphiphiles Self-Assemble into Stable Primitive Membranes in Diverse Geological Settings

Trishool Namani,[1] Reghan J. Ruf,[1,2] Iskinder Arsano,[1] Ruibo Hu,[1] Chrys Wesdemiotis,[1,3] and Nita Sahai[1,2,4,5]

Abstract

Primitive cells are believed to have been self-assembled vesicular structures with minimal metabolic components, that were capable of self-maintenance and self-propagation in early Earth geological settings. The coevolution and self-assembly of biomolecules, such as amphiphiles, peptides, and nucleic acids, or their precursors, were essential for protocell emergence. Here, we present a novel class of amphiphiles—amino acid-fatty alcohol esters—that self-assemble into stable primitive membrane compartments under a wide range of geochemical conditions. Glycine *n*-octyl ester (GOE) and isoleucine *n*-octyl ester (IOE), the condensation ester products of glycine or isoleucine with octanol (OcOH), are expected to form at a mild temperature by wet-dry cycles. The GOE forms micelles in acidic aqueous solutions (pH 2–7) and vesicles at intermediate pH (pH 7.3–8.2). When mixed with cosurfactants (octanoic acid [OcA]; OcOH, or decanol) in different mole fractions [$X_{\text{Cosurfactant}} = 0.1$–$0.5$], the vesicle stability range expands significantly to span the extremely acidic to mildly alkaline (pH 2–8) and extremely alkaline (pH 10–11) regions. Only a small mole fraction of cosurfactant [$X_{\text{Cosurfactant}} = 0.1$] is needed to make stable vesicular structures. Notably, these GOE-based vesicles are also stable in the presence of high concentrations of divalent cations, even at low pHs and in simulated Hadean seawater composition (without sulfate). To better understand the self-assembly behavior of GOE-based systems, we devised complementary molecular dynamics computer simulations for a series of mixed GOE/OcA systems under simulated acidic pHs. The resulting calculated critical packing parameter values and self-assembly behavior were consistent with our experimental findings. The IOE is expected to show similar self-assembly behavior. Thus, amino acid-fatty alcohol esters, a novel chimeric amphiphile class composed of an amino acid head group and a fatty alcohol tail, may have aided in building protocell membranes, which were stable in a wide variety of geochemical circumstances and were conducive to supporting replication and self-maintenance. The present work contributes to our body of work supporting our hypothesis for synergism and coevolution of (proto)biomolecules on early Earth. Key Words: Amino acid-fatty alcohol ester amphiphile—Primitive membrane—Extreme pH—Divalent cations—Seawater—Vesicle. Astrobiology 23, xxx–xxx.

[1]School of Polymer Science and Polymer Engineering, University of Akron, Akron, Ohio, USA.
[2]Integrated Biosciences Program, University of Akron, Akron, Ohio, USA.
Departments of [3]Chemistry, [4]Geosciences, and [5]Biology, University of Akron, Akron, Ohio, USA.

1. Introduction

The modern cell membrane is composed of a complex mixture of phospholipids, which comprise the lipid bilayer, as well as proteins, which play crucial roles in maintaining the structural and functional integrity of cells (Harayama and Riezman, 2018). Phospholipids, which have a cylindrical shape and a critical packing parameter (cpp) of ~ 1, consist of a glycerol phosphocholine headgroup with two fatty acyl chains and form self-assembled, spherical bilayer membrane structures (vesicles) when dispersed in aqueous solution (Israelachvili *et al.*, 1977).

Phospholipid vesicles are stable under a wide range of pH, monovalent salt concentration, and temperature ranges, which allows them to persist across a plethora of geological settings. These vesicles are also useful in the pharmaceutical industry as drug carriers (Beltrán-Gracia *et al.*, 2019). However, phospholipids are generally considered to be prebiotically less probable because their synthesis would require complex enzymatic pathways that would not have existed during the formation of the first protocells.

This limited prebiotic plausibility of molecules that form stable cell membranes over a wide range of geochemical solution compositions presents a challenge in origins of life research. Although notable attempts to overcome this problem do exist (Hargreaves *et al*., 1977; Rao *et al*., 1982; Rao *et al.*, 1987; Maheen *et al.*, 2010; Patel *et al*., 2015), the simulated experimental settings beg further refinement or even modification (Bonfio *et al.,* 2019).

Further, ions and solutes cannot easily pass through pure phospholipid membranes because they are highly impermeable; in modern cells, nutrients are taken in and waste is disposed of through a sophisticated enzymatic process and membrane channels or pumps, but this complex transport machinery would not have existed during the formation of the first protocells (Mansy, 2010).

Fatty acid-based vesicles have long been regarded as models for prebiotic membranes (Szostak *et al.,* 2001; Monnard *et al.*, 2002; Chen *et al.*, 2005; Dalai and Sahai, 2018, 2019a; Dalai *et al*., 2018). Chemically simple, able to form in presumably prebiotic conditions, and found in exogenous materials, fatty acids are attractive as the fundamental building block of protocell membranes (Deamer, 1985; Deamer and Dworkin, 2005; Ruiz-Mirazo *et al*., 2014; Dalai *et al.*, 2016, 2018; Dalai and Sahai, 2019b).

Fatty acid vesicles exhibit intriguing physical properties such as growth (Berclaz *et al.*, 2001; Chen and Szostak, 2004), self-reproduction (Hanczyc *et al.,* 2003; Luisi *et al*., 2004), and a primitive form of competition (Chen *et al*., 2004; Stano, 2007). Pure fatty acid vesicles, though, are limited in their application as protocell membranes because they are susceptible to structural modification in response to variations in pH, temperature, and the presence of high concentrations of monovalent salts as well as low concentrations of divalent salts (Cistola *et al.*, 1988; Deamer *et al*., 2002; Namani and Walde, 2005; Monnard and Walde, 2015; Maurer and Nguyen, 2016).

As recently shown, concentrations of divalent Mg^{2+} could vary from the millimolar range in komatiite weathering freshwater solutions to sub-micromolar in evaporative brine solutions, due to Mg^{2+}-silicate and -carbonate mineral precipitation on Hadean Earth (Sahai *et al.*, 2022). These changes in self-assembly behavior represent a long-standing roadblock in building a robust, prebiotically plausible protocell that is stable across numerous geological settings. Importantly, various cosurfactants, such as fatty alcohols (Apel *et al.*, 2002; Jordan *et al.*, 2019b), fatty acid glycerol esters (Apel and Deamer, 2005; Simoneit *et al.*, 2007), fatty amines (Namani and Deamer, 2008; Maurer *et al.*, 2018), cyclophospholipids (Toparlak *et al.*, 2020), and phospholipids (Dalai and Sahai, 2018), can be used to stabilize the vesicles, though these cosurfactants present their own challenges.

In detail, the admixture of fatty alcohol to fatty acid produces vesicles, which are stable under alkaline conditions, but not stable in the presence of divalent cations, such as Mg^{2+} and Fe^{2+}, that are required for RNA template-mediated RNA polymerization reactions (Dalai and Sahai, 2018). Similarly, admixtures of fatty acids with fatty amines give rise to vesicles that show remarkable stability toward divalent cations, but the prebiotic relevance of fatty amines remains in question (Namani and Deamer, 2008).

Vesicle membranes composed of fatty acid-phospholipid mixtures are stable up to high concentrations of divalent cations because the cations bind and abstract the fatty acid from the membrane, thus relatively enriching the membrane in phospholipids compared with its original molar composition (Dalai *et al.*, 2018); however, as noted earlier, the abundance of phospholipids on early Earth may have been limited (Dalai and Sahai, 2018). Several recent studies have concentrated on producing vesicles containing a variety of single chain amphiphile mixtures, including isoprenoids (Jordan *et al.*, 2019a), and sometimes even a mixture of four amphiphiles (Sarkar *et al.*, 2020), that are immune to divalent cations and exhibit stability over a larger pH range (Maurer *et al.,* 2018).

Most of these discoveries are centered on stabilizing vesicles under alkaline pH conditions, however, and little study has been done on constructing vesicles from prebiotically plausible amphiphiles that can withstand both acidic pH and divalent cations, or indeed a wide range of pHs. Particularly overlooked in the construction of primitive membranes is the potential role of amino acids.

Prebiotic biomolecules are believed to have coevolved as a result of various geological and environmental factors, where temperature, pH, salinity and the presence of divalent cations served as selection pressures (Kaddour and Sahai, 2014; Sahai *et al*., 2016; Dalai *et al*., 2018; Frenkel-Pinter *et al*., 2020; Namani *et al.*, 2021). Chemical evolution involves the mutual interaction of a large number of prebiotically plausible molecules to produce robust biomolecules or their precursors, and selection of those specific molecules under environmental selection pressures, over a wide range of geological conditions.

We have previously hypothesized that mutualism and coevolution of biomolecules such as lipids, amino acids, and nucleotides, or their precursors as catalyzed by minerals and dissolved metal ions, may have spurred protocell evolution (Kaddour and Sahai, 2014; Sahai *et al.*, 2016, 2017; Dalai and Sahai, 2018; Dalai *et al.*, 2018; Kaddour *et al*., 2018; Dalai and Sahai, 2019a, 2019b; Zhou *et al.*, 2020; Namani *et al*., 2021). These selection pressures, in turn, lead to the formation of modern biomolecules, such as peptides, nucleic acids, and lipids.

Amino acids play crucial roles in prebiotically relevant processes, such as promotion of nonenzymatic, montmorillonite-catalyzed RNA polymerization (Namani *et al*., 2021). Amino acids can also stabilize fatty acid membrane compartments (Cornell *et al*., 2019) and nucleobases can interact strongly with fatty acid membranes, thus showing how biomolecules may have interacted with protocells (Black *et al.*, 2013). Recently, Bonfio *et al*. (2020) demonstrated the synthesis of *N*-decanoyl arginine from mixtures of amino acids and *N*-acylated amino acids exposed to activation conditions, but the self-assembly behavior of these amphiphiles was not examined.

Including amino acids in the discussion of protocell membrane compositions could potentially resolve the limitations presented by traditional fatty acid membranes with cosurfactants of fatty alcohols, fatty amines, or fatty acid glycerol esters. Thus, we hypothesized in the present study that: (i) commonly occurring prebiotic molecules, amino acids and fatty alcohols, could undergo esterification reactions under near-equilibrium, moderate-temperature wet-dry cycles; (ii) at acidic pH, the amine-head group of the resulting ester amphiphiles would form stable vesicles; and (iii) mixtures of these amino acid-fatty alcohol esters with fatty acid or fatty alcohol amphiphiles would generate stable vesicles over a wide range of pH, salinity, and divalent cation conditions representing diverse geochemical environments.

In our current work, we present one such scenario in which prebiotically plausible amino acids and amphiphiles work together to form a novel class of molecular chimera, amino acid-fatty alcohol esters. Specifically, we studied glycine *n*-octyl ester (GOE) and isoleucine *n*-octyl ester (IOE) formed by the condensation of glycine or isoleucine and octanol (OcOH), respectively (Fig. 1a). Both amino acids and fatty alcohols are prebiotically plausible (*i.e.,* they are chemically simple and are found in meteorites) (Sephton, 2002), and the corresponding esters are shown here to be tentatively synthesized under geologically realistic wet-dry conditions. The objectives of this study, then, were as follows: (i) to synthesize GOE and IOE by simple wet-dry cycles at moderate temperatures; (ii) to examine whether pure GOE can form vesicles; (iii) to investigate how the pH range of GOE-based vesicles can be extended by mixing cosurfactants octanoic acid (OcA), OcOH, or decanol (Fig. 1a); (iv) to explore the effects of divalent cations and seawater on amphiphile self-assembly behavior; and (v) to examine whether experimental observables that are computationally quantifiable via cpp values from molecular dynamic (MD) simulations can accurately explain the self-assembly behavior of mixed amphiphile systems.

Taken together with our previous work, we add evidence here to our hypothesis that biomolecules or their precursors coevolved, rather than appearing sequentially, and that this process was promoted by the specific minerals and dissolved ions present in the environment on Hadean Earth (Kaddour and Sahai, 2014; Sahai *et al*., 2016, 2017; Dalai and Sahai, 2018; Dalai *et al.,* 2018; Kaddour *et al*.., 2018; Dalai and Sahai, 2019a, 2019b; Zhou *et al.*, 2020; Namani *et al.*, 2021; Sahai *et al.*, 2022).

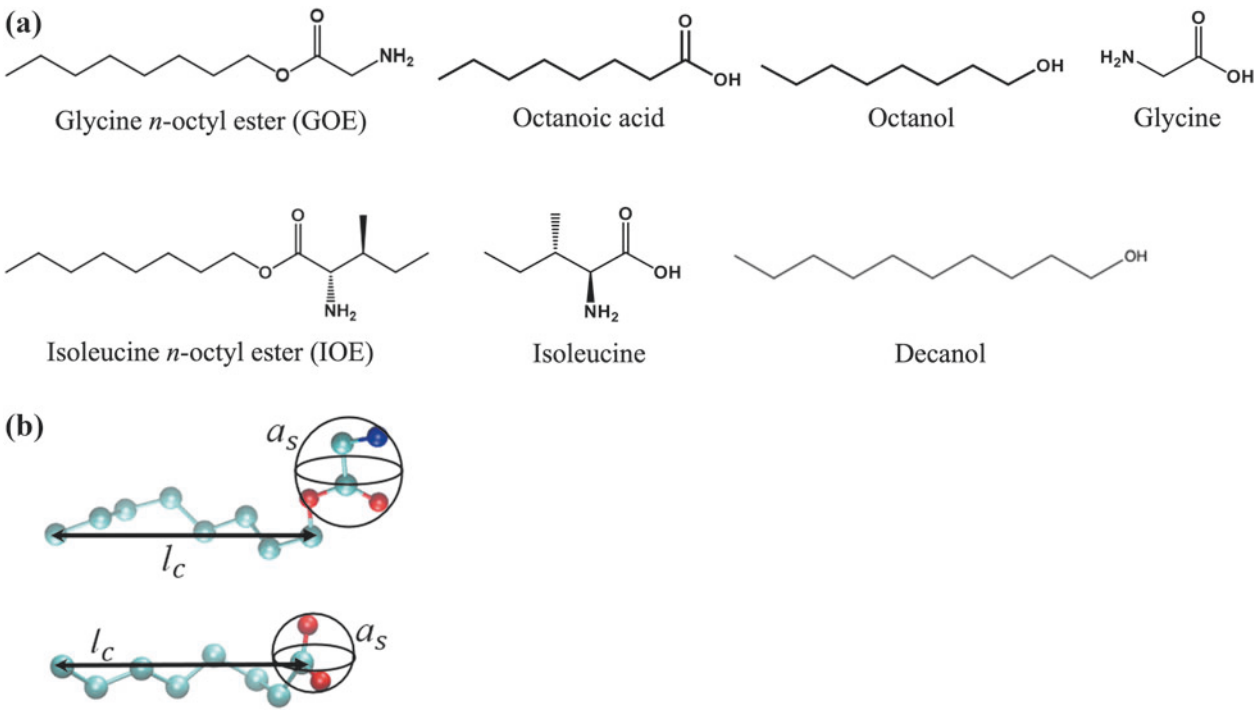

FIG. 1. **(a)** Chemical structures of GOE, OcA, OcOH, glycine, IOE, isoleucine, and decanol. **(b)** Vacuum-relaxed structures of GOE (top) and OcA (bottom) obtained by molecular dynamics simulations. The double-headed arrow indicates the alkyl chain length (l_c) for each amphiphile, and the sphere bounded by black circles indicates the head group surface area (a_s) used for calculating the cpp of each molecule. Cyan = carbon, red = oxygen, and blue = nitrogen atoms. cpp = critical packing parameter; GOE = glycine *n*-octyl ester; IOE = isoleucine *n*-octyl ester; OcA = octanoic acid; OcOH = octanol.

2. Materials and Methods

2.1. Materials

All reagents (>99% pure) were obtained from Sigma® or Fisher Scientific® unless otherwise noted. Glycine *n*-octyl ester hydrochloride (GOE.HCl), *n*-octanol, and *n*-octanoic acid were purchased from Thermo Scientific (Rockford, IL) (purity >99%). A mixture of modern ''seawater'' composition (NaCl 24.53 g/L, $MgCl_2 \cdot 6H_2O$ 5.20 g/L, $CaCl_2$ 1.16 g/L, KCl 0.695 g/L, Na_2SO_4 4.09 g/L, $NaHCO_3$ 0.201 g/L, KBr 0.101 g/L, H_3BO_3 0.027 g/L, $SrCl_2 \cdot 6H_2O$ 0.025 g/L, and NaF 0.003 g/L) was purchased from Lake Products Company LLC (MO), and the reconstitution of modern seawater was done according to the manufacturer's instructions.

Separately, individual salts of the same composition (excluding sodium sulfate) were mixed in identical concentrations as the modern sea salts to prepare simulated Hadean seawater. The simulated modern and Hadean seawater had pH of ~8. All solutions were made using ultrapure water (~18.2 MΩ-cm, Barnstead™ GenPure™ xCAD Plus; Thermo Scientific).

2.2. Acid-base titration curves

By combining a defined amount of commercial GOE.HCl with water, a micellar stock solution of GOE (0.2 *M*) was prepared (initial pH = ~4). A series of glass vials (4 mL) were filled with 0.5 mL GOE micelles (0.2 *M*) aliquots, titrated with different concentrations of NaOH (1 *M*) up to pH ~11, and the final volume was adjusted to 1 mL with water. After brief vortexing, the pH of each sample was measured using a pH electrode (Mettler Toledo InLab®) and the pH versus NaOH concentration was plotted to obtain a titration curve.

Similarly, acid-base titration curves were prepared for the following systems with a total amphiphile content of 0.1 *M*: GOE/OcA 1:1 [$X_{GOE} = 0.5$, $X_{OcA} = 0.5$], initial pH = ~3 and 3:1 [$X_{GOE} = 0.75$, $X_{OcA} = 0.25$], initial pH = ~3.5; GOE/OcOH 1:1 [$X_{GOE} = 0.5$, $X_{OcOH} = 0.5$], initial pH = ~4.5 and 3:1 [$X_{GOE} = 0.75$, $X_{OcOH} = 0.25$], initial pH = ~4; and GOE/decanol 1:1 [$X_{GOE} = 0.5$, $X_{Decanol} = 0.5$], initial pH = 4.5. Additional experiments were performed to confirm that GOE does not hydrolyze into glycine and OcOH at extreme alkaline pH >10 (see SI 1 section in Supporting Information).

2.3. Continuous variation samples in GOE/cosurfactant systems

Continuous variation (CV) graphs, or ''Job plots,'' are commonly used in analytical chemistry to determine the stoichiometry of aqueous complexes, such as metal-ligand complexes (Cantor and Schimmel, 1980; Job, 1928). Here, we prepared CV samples to determine the ratios at which commercial GOE.HCl and cosurfactants, OcA or OcOH, form vesicles. The total concentration of lipid was 0.1 *M* in a series of solutions, whereas mole fractions of GOE and OcA or OcOH were varied from 1.0 to 0.0 and 0.0 to 1.0, respectively. All samples were prepared in ultrapure water with a final pH of 3–4. All samples were analyzed by light microscopy.

2.4. Microscopy analysis

All GOE and GOE/cosurfactant samples were observed under an inverted light microscope (Olympus IX51; Olympus America, Inc., Melville, NY) using a 100× oil objective lens to investigate the presence of vesicles. Images were recorded with a QImaging sCMOS camera (optiMOS, Surrey, BC, Canada) and viewed with cellSens Dimension 1.7 software.

For select systems, vesicles were stained with perylene (0.025 mol %), a fluorescent hydrophobic polyaromatic hydrocarbon, and imaged using epifluorescence microscopy (see SI 1 section in Supporting Information). A mercury pressure short-arc lamp HBO 103 W/2 (OSRAM, GmbH) was used as the light source, and an ultraviolet (DAPI) filter set was used for the epifluorescence microscopy. All images were taken at room temperature. ImageJ software was used to adjust brightness and contrast to optimize images. Additional details regarding the preparation of vesicles stained with perylene are provided in SI 1 section in Supporting Information.

2.5. Experimental GOE and IOE synthesis

The GOE and IOE wet-dry synthesis experiments were carried out using a 9-cavity electron microscopy sciences Pyrex™ plate (the semispherical cavity is 1/4″ [6.4 mm] deep with a 7/8″ [22 mm] diameter) in an anaerobic glove bag under normal atmospheric pressure and pH 7. To synthesize GOE, 0.5 mL of 0.1 *M* glycine and 8 μL of 0.1 *M* OcOH (1:1 mole ratio) were added in each cavity of the 9-cavity Pyrex plate. Two identical plates were prepared, one of which was heated to a temperature of 50°C and the other to 80°C using hot plates (Echotherm™ Orbital Mixing Chilling/Heating Dry Bath; Torrey Pines Scientific, Inc.®, Carlsbad, CA, Standard Heatblock; VWR® Scientific Products, Radnor, PA).

After the initial glycine/OcOH 1:1 mixture had dried down completely, a volume of 0.5 mL ultrapure water was added to each cavity every 3 h for a total of three wet-dry cycles over a period of 9 h. In a separate synthesis experiment, we performed only one wet-dry cycle under otherwise identical conditions where only the initial glycine/OcOH 1:1 mixture was dried down. All samples were dried down completely during each wet-dry cycle. The resulting products were then either collected as solid samples or diluted in 0.5 mL ultrapure water, centrifuged for 5 min at 13,500 rpm, and the supernatants were collected.

The same procedure was repeated for synthesis of IOE using three 3 h wet-dry cycles (isoleucine *n*-octanoyl ester). The GOE and IOE synthesis products were then analyzed by electrospray ionization–mass spectrometry (ESI-MS) and tandem ESI-MS ($ESI\text{-}MS^2$).

2.6. ESI-MS analysis

Working solutions were prepared by dissolving solid samples directly in acetonitrile (ACN) to precipitate out any unreacted glycine or by diluting supernatant stock solutions 10× into 2-propanol (Optima LC-MS grade; Fisher Chemicals®), filtered with ARCODISC® 13 mm disks with 0.2 μm pore size PTFE membrane filters, then diluted again by a factor of 100× into ACN before direct injection. ESI-MS analyses were performed on a Bruker© HCTultra™ II Quadrupole Ion Trap (Bruker Daltonics, Billerica, MA) equipped with ESI, operated in both positive and negative ionization mode.

The target mass was set to *m/z* 150 for all experiments to optimize product ion intensity; therefore, relative ion intensities are not considered quantitative. Nebulizing pressure and flow were set to 10 psi and 8 L/h, respectively, and the dry gas temperature was maintained at 300°C. Maximum ion accumulation time in the trap cell was 200 ms, and spectra were acquired over a 2-min period. Reaction products were analyzed via ESI-MS^2 and compared against a commercial standard, GOE.HCl, which was subjected to identical conditions (see SI 2 section and Supplementary Table S1 in Supporting Information).

Additional details on these experiments can be found in SI 2 section in Supporting Information. All spectra were background-subtracted by defining the dwell volume of the previous solvent preceding solvent blank as background. Bruker esquireControl© v6.2 was used for data acquisition, and Compass DataAnalysis© v4.0 software was used for the analysis.

2.7. MD simulations

The MD simulations were conducted at the Ohio Supercomputer Center to study the self-assembly behavior of a series of mixed GOE/OcA systems at different mole fractions corresponding to the experimental systems at acidic pH (<3.5) (see SI 3 section in Supporting Information). The average shape of the molecule (length of fatty carbon tail, l_c, and surface area of headgroup, a_s) was used to calculate cpp values (Fig. 1b).

The cpp values can be used to predict the self-assembly behavior of the amphiphiles to form micelles, vesicles, or oil-phase (see Section 2.8) and to obtain molecular density maps of the amphiphiles in water. All the simulated systems are created to represent a pH <3.5, in which all the molecules are simulated with protonated carboxyl groups (*i.e.,* in the nonionized form). These are analogous to our experimental systems where the HCl salt of GOE was used, which results in a solution pH <4 even in the case of 100% GOE (corresponding to experimental system 0.1 *M*).

Chloride ions were used in the MD simulations to maintain overall neutral charge in all GOE-containing systems to balance the excess positive charge arising from the protonated amine moieties. Two main types of molecular systems were examined, based on the number of amphiphiles in the system, as described later in greater detail (also see SI 3 section in Supporting Information).

In one type of molecular system, *multiple* amphiphile molecules with explicit water molecules were examined at various mole fractions of octanoic acid (X_{OcA}) to obtain (i) the average shape of the molecule and to calculate cpp; and (ii) qualitative estimates of self-assembly behavior by calculating amphiphile density maps (see Section 2.9). In this explicit solvation computational system, a pure water starting configuration of 33,456 molecules was generated using CHARMM GUI software (Jo *et al.,* 2008).

This water system has a periodic cubic dimension of 10 nm^3. The GOE and OcA molecules were relaxed in vacuum using Avogadro software (Hanwell *et al.*, 2012) and were replicated, randomly dispersed in the water system, and arranged in five separate systems of various X_{OcA} values with cubic dimension 10 nm^3 for each system. All five X_{OCA} systems contained a total amphiphile concentration of 0.1 *M*, with varying X_{OcA} values = 0.0, 0.10, 0.5, 0.9, or 1.0. The total amphiphile count in each X_{OcA} system is 60, and the total water count is 33,456 (see SI 3 section and Supplementary Table S2 in Supporting Information).

In the second type of molecular system, the geometry of a *single* amphiphile molecule (GOE or OcA) was analyzed in two environments, namely, vacuum and in implicit solvent, and the shape of the molecule from each solvation environment was used to calculate cpp values (Fig. 1b, see Sections 2.8–2.9, and SI 3 section in Supporting Information). Single GOE and OcA molecules (both in their protonated forms) were individually relaxed in vacuum using Avogadro software (Hanwell *et al.*, 2012). The simulations were allowed to run for 125 ps to collect information on how the molecule shape changes in vacuum over time.

The shape information was then used to calculate cpp values and corresponding standard deviation errors. Separate analogous implicit solvent (dielectric constant = 78.39) relaxations were also performed on Q-CHEM quantum chemistry software (Shao *et al.*, 2015) to obtain a cpp value for a single GOE or a single OcA molecule.

CHARMM-36 (MacKerell Jr. *et al.*, 1998) force field was used for the amphiphiles and ions. Transferable intermolecular potential with three points (Jorgensen *et al.*, 1983) water model was used for water molecules. GROMACS (Bekker *et al.*, 1993; Berendsen *et al.*, 1995) software package was used for both energy minimization and production runs. A steepest descent algorithm was used over 5000 steps to achieve energy minimization. After 125 ps of system equilibration using the canonical thermodynamic ensemble (constant number, volume, and temperature), a total of five (each 0.025 μs long) NPT (constant number, pressure, and temperature) production simulations were computed.

A time step of 1 fs was used for the equilibration run with trajectory data collection every 5 ps, and a time step of 2 fs with trajectory data collection every 20 ps was used for the production run. A short-range nonbonded interaction cut-off distance of 1.2 nm was used. Long-range electrostatic interactions were accounted for using the Particle-mesh Ewald calculation scheme (Darden *et al.*, 1993).

2.8. cpp Estimation

The cpp determines the type of amphiphilic self-assembled structure that can form based on the geometry of the amphiphile molecule under the existing solution conditions. The cpp is calculated as (Ramanathan *et al*., 2013):

$$\text{cpp} = \frac{v_c}{l_c a_s} \tag{1}$$

where v_c is the volume (nm^3) of the extended alkyl chain; l_c is the length of the extended alkyl chain (nm); and a_s is the surface area (nm^2) occupied by an amphiphilic molecule at the molecule-water interface (Fig. 1b). For mixed amphiphile GOE/OcA systems at various values of X_{OcA}, the cpp values of the overall system were calculated as a molar weighted average of the individual GOE and OcA molecules in each corresponding system (see SI 3 section and Equations S1–S3 in Supporting Information).

Values of cpp < 0.5 are indicative of formation of micelles, whereas large values of cpp > 1 correspond to the formation of reverse micelles or aggregates of reverse

micelles (seen visually as phase-separated ''oil droplets'' or as a separate oil layer floating on an aqueous layer). Vesicles are observed at intermediate values < 0.5 cpp < 1 (Ramanathan *et al.*, 2013).

Here, l_c is estimated as the distance between the centers of mass of the first and last carbon atoms belonging to the alkyl chain of the specific amphiphile molecule, and a_s is determined as the surface area of the sphere whose diameter is the maximum separation between any pair of molecules in the hydrophilic head group (Fig. 1b). The a_s values reported here are for the amphiphile molecules, including only the heteroatoms (see SI 3 section in Supporting Information).

Alternatively, in the absence of a reliable way of measuring amphiphile tail sizes, one may use an approximation of constant l_c based on the empirical relationship (Ramanathan *et al.*, 2013):

$$l_c \sim 80\ \%\ \text{of}\ (0.154\ +\ 0.1265\ n) \tag{2}$$

where n is the number of carbons in the hydrophobic tail and l_c is in units of nm.

Alkyl chain volume, v_c (in units of nm^3) can be estimated as (Ramanathan *et al.*, 2013):

$$v_c = (27.4\ +\ 26.9\ n) * 10^{-3}$$

The change of shape of amphiphile molecules over the period of the production run was recorded to obtain standard deviation errors for the calculated values. The standard deviation error for cpp values was calculated to reflect the time change of cpp values with respect to calculated averages. Accordingly, the error margin for single amphiphile molecules in vacuum is within 2.1% and is within 0.06% for the major explicit solvent (water-ion-amphiphile) simulations. Errors are not available for the single molecule implicit solvent relaxations, as a cpp value each for GOE and OcA was obtained. Results of the calculation are provided in Supplementary Tables S3–S6 for the three types of molecular systems considered.

2.9. Amphiphile density maps for explicit solvation systems

Grid-based three-dimensional amphiphile density maps were created for all five X_{OcA} simulation systems based on average amphiphile positional data from the explicit solvent production runs. A cubic grid of $1\,nm^3$ was used to bin positional information. The binned amphiphile density value in each grid point (bin) was differentiated into high-density (bright colors) and low-density (dim colors) regions. For ease of visual analysis, the density distribution in the simulation box was categorized by percentiles. This was done separately for each amphiphile species, and in each of the five X_{OcA} explicit solvent simulation systems.

More than half of the mass was found to occupy patches of the simulation box with the top 80% of density values. These patches were visualized as high-density regions where substantial molecular association occurs. The remaining patches were taken as low-density regions where molecules are only loosely associated. This allowed a qualitative characterization of the nature of self-assembly as the system responded to changes in mixed amphiphile composition in the simulated low pH environment.

3. Results

3.1. Experimental GOE and IOE synthesis

The first goal of our study was to examine whether GOE or IOE could be synthesized from glycine or isoleucine and OcOH under prebiotically plausible conditions. We combined amino acid and OcOH in a 1:1 mole ratio under anaerobic conditions and performed one to three 3-h wet-dry cycles, for a total of 3 or 9 h, respectively, at temperatures of 50°C and 80°C. The ESI-MS results reveal the tentative formation of protonated GOE at *m/z* 188.1 at 50°C but not at 80°C (Supplementary Figs. S1a, c and S3 and Supplementary Table S1).

The ESI-MS spectrum at 80°C showed a peak at *m/z* 137, which is consistent with the formation of piperazine-2,5-dione, a cyclic glycine dimer, that may have prevented the formation of our target product, GOE (Supplementary Figs. S1c and S3 and Supplementary Table S1). The spectrum at 80°C also showed a peak at *m/z* 83, which is consistent with the deamination of glycine (Supplementary Figs. S1c and S3 and Supplementary Table S1).

The ESI-MS results for the synthesis of IOE reveal the formation of the sodiated form of IOE (IOE-Na^+ noncovalently bound cluster) at *m/z* 266 at $T = 50$°C condition but not at 80°C (Supplementary Figs. S1b, d and S3 and Supplementary Table S1). The ESI-MS spectrum at 80°C showed peaks at *m/z* 132 and 154, which are consistent, respectively, with Ile+H^+ and Ile+Na^+; *m/z* 176, corresponding to Ile-H^+ + 2Na^+; and a peak at *m/z* 285, which may be assigned to a sodium-bound dimer of Ile (Supplementary Figs. S1d and S3 and Supplementary Table S1).

Further structural characterization was performed on an additional GOE synthesis sample, where sample product ions were analyzed via ESI-MS^2 and compared with commercial reference material (GOE.HCl) under both positive and negative ionization potentials. The ESI-MS revealed ions at *m/z* 188 and 210, which are interpreted as GOE species, $[M+H]^+$ and $[M+Na]^+$, respectively (Supplementary Fig. S4a). The ion at *m/z* 210 was able to be isolated more efficiently as a monoisotopic ion for subsequent ESI-MS^2, so it was selected for collisionally activated dissociation (CAD) (Supplementary Fig. S4b).

Subjecting that ion (*m/z* 210) to CAD revealed significantly more peaks, suggesting the formation of additional ions in the mixture. In detail, the *m/z* 210 peak may be an isomer of GOE, octylglycine (Supplementary Figs. S3a and S4c-I). In comparison, the *m/z* 210 peak in ESI-MS^2 of the commercial GOE standard was relatively stable under the activating conditions, and it revealed only one peak (*m/z* 193) corresponding to a neutral mass loss of 17 (M-17), resulting in $[M\text{-}NH_3 + Na^+]^+$ (Supplementary Fig. S5). This M-17 peak was also observed in the synthesized putative GOE sample spectrum (Supplementary Fig. S4c).

Additional fragments M-16 (*m/z* 194) and M-18 (*m/z* 192) were also present (Supplementary Fig. S4c). The mass loss of 16 could possibly be due to a resonance-stabilized distonic radical formed via homolytic cleavage at the α-carbon of the N-terminus of glycine. The neutral mass loss of 18 suggests the liberation of a water molecule. This reaction is more likely to occur for a carboxylate headgroup—as found

in octylglycine—rather than for an ammoniated headgroup, as found in GOE. The octylglycine isomer could potentially have formed via an S_N2 reaction to alkylate the primary amine of glycine.

The peak at *m/z* 164 (M-46) most likely resulted from a neutral mass loss of formic acid, resulting in the formation of a sodiated amine $[M - CH_2O_2 + Na^+]^+$ (Supplementary Fig. S4c). The peak at *m/z* 98 observed in the synthesized GOE spectrum is assigned to sodiated glycine, due to neutral mass loss of octane (M-114) (Supplementary Fig. S4c). This product could form from a known rearrangement of esters involving six e^- transfers (McLafferty, 1959). Importantly, the presence of the *m/z* 98 peak provides evidence for covalent linkage of glycine on the isolated product in our synthesized sample.

To further investigate the possibility of carboxylate isomers—such as octylglycine—being present in the mixture, a small fraction of the synthesized GOE was analyzed by ESI-MS using negative ionization mode and compared against the commercial standard (Supplementary Fig. S6). Given that commercial GOE does not have a readily acidic proton, it is unlikely to ionize in negative mode (Supplementary Fig. S6a). The synthesized sample spectrum, however, revealed the presence of an ion at *m/z* 186, which is suggestive of the presence of carboxylate isomeric species that are observed as $[M\text{-}H]^-$ (Supplementary Fig. S6b).

These results are consistent with the preceding ESI-MS^2 spectrum obtained for the sodium bound monomer $[M+Na^+]^+$ (*m/z* 210), which revealed the isomeric and/or isobaric mixture of compounds present when compared with the fragments observed in the commercial GOE spectrum (Supplementary Figs. S4c and S5).

In summary, both GOE and IOE were *tentatively* formed by wet-dry cycling at 50°C but were not observed at 80°C.

3.2. Titration experiments

Our next objective was to investigate whether pure GOE.HCl can form vesicles in an aqueous solution. To test this, we performed a simple acid-base titration experiment on pure commercial GOE (0.1 *M*, pH ~3–4) using 1 *M* NaOH and the resulting titration samples were then analyzed by eye and with epifluorescence microscopy to examine self-assembly behavior (Fig. 2a, b, e). The pure GOE samples formed clear solutions, suggesting micelle formation up to pH 7.3 (Fig. 2b). At pHs between pH 7.3 and 8.2, the samples became turbid, suggesting phase transformation to stable vesicles in this pH range (Fig. 2a, b, e).

Above pH 8.7, the suspension separated into two liquid phases: an aqueous phase and an oil phase (Fig. 2a, b). The pK_a of the amine group in GOE is ~9.5; however, the titration curve shows an apparent pK_a ~8 (50% of 0.1 *M* GOE ionization at 0.05 *M* NaOH) for GOE when present in the vesicle membrane (Fig. 2a). In summary, pure GOE can, indeed, form stable vesicles in aqueous solution at pHs 7.3–8.2 (Fig. 2b).

Our next objective was to explore various GOE/cosurfactant (OcA and OcOH) mixtures to establish a wider pH range for stability of GOE-based vesicles (Figs. 2 and 3). At a GOE/OcA 1:1 mole ratio [$X_{GOE} = 0.5$, $X_{OcA} = 0.5$] and pH 3, the samples became turbid, indicating that vesicles form at acidic pH, which was confirmed by light microscopy (Figs. 2a, c, and 3a). These vesicles are even stable at extremely acidic conditions in the presence of 0.01 *M* HCl, pH 2 (Fig. 2f). When NaOH was added to obtain pHs ~4–5, the suspensions turned milky white—indicating the presence of oil droplets—which was confirmed by microscopy analysis (Figs. 2c and 3a).

Between pH ~6–8.2, the samples phase-separated (Figs. 2c and 3a). At pH >10, the mixture became turbid once again, suggesting the re-formation of vesicles (Figs. 2c and 3a). This is a significant result, because it expands the stability range of GOE-based cosurfactant systems over a very wide pH range. However, it is possible that the vesicles observed at such high pHs are formed by octanoic acid and octanol, where the latter was produced by base-catalyzed GOE hydrolysis into OcOH and glycine.

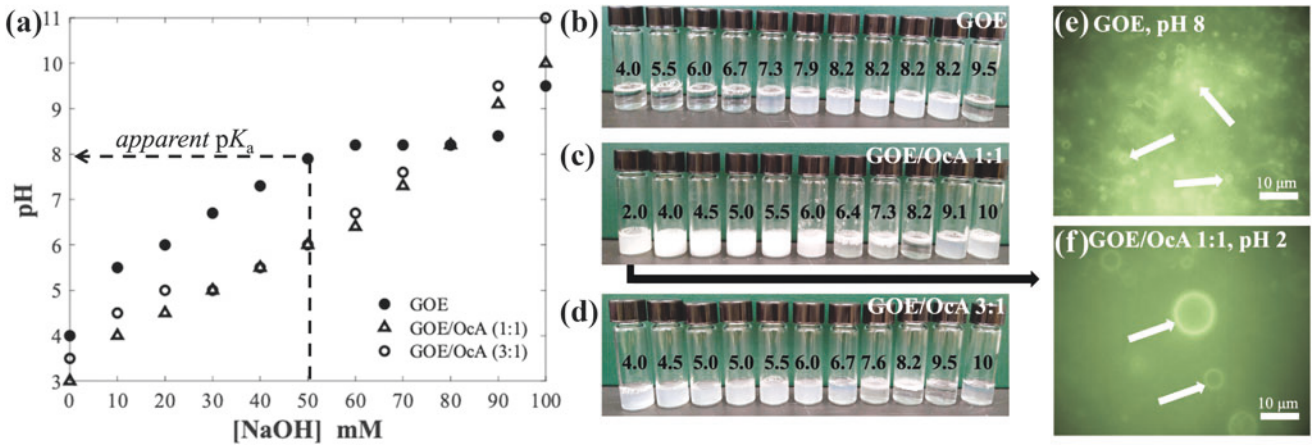

FIG. 2. pH-dependent self-assembly of GOE/OcA cosurfactant systems. **(a)** Equilibrium pH titration curve, where the dashed line represents the apparent pK_a of GOE, corresponding to 50% ionization (0.05 *M* NaOH); **(b–d)** the corresponding sample vials for the pH titrations, where the numbers on the vials indicate solution pH; photomicrographs of **(e)** pure GOE vesicles, pH 8, and **(f)** GOE/OcA (1:1) vesicles prepared in 0.01 *M* HCl suspension, pH 2. The black arrow from panel **(c)** to panel **(f)** points from the bulk sample at pH 2 to the corresponding photomicrograph. Perylene, a lipophilic dye molecule, was used (0.025 mol %) for visualization of the vesicle structures, which are indicated by solid white arrows. Total lipid concentration = 0.1 *M*.

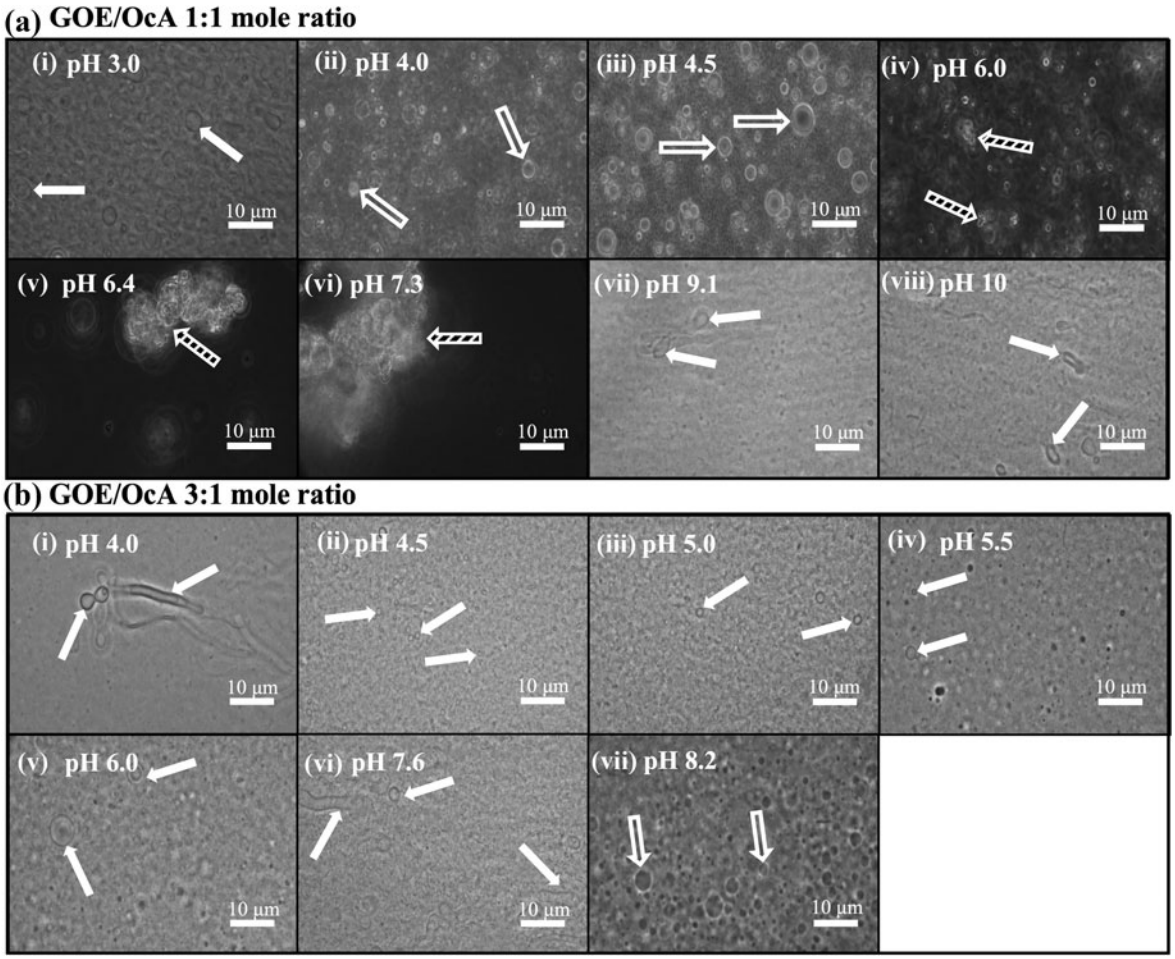

FIG. 3. Photomicrographs of GOE/OcA 1:1 mole ratio **(a)** and 3:1 mole ratio **(b)** acid-base titration samples from Figure 2c, d. Solid white arrows indicate vesicles, hollow white arrows indicate oil droplets, and black/white striped arrows indicate phase-separated aggregates. Total lipid concentration = 0.1 *M*.

To further examine the possibility of base-catalyzed GOE hydrolysis, we conducted a separate GOE titration experiment. A series of samples containing 0.1 *M* commercial GOE was titrated to pH 10 with 1 *M* NaOH and showed phase-separation (Supplementary Fig. S7a, b); after incubating for 2 h, all the samples were back-titrated with 1 *M* HCl to their starting pH of 3.5 and all these samples transitioned back to clear solutions, indicating micelle formation, with the addition of HCl (Supplementary Fig. S7a–c).

This could occur only if most of the GOE was intact at pH 10. Analysis by ^{1}H NMR confirmed that at pH 10, GOE was largely still intact, though a small amount ($\sim$10%) of OcOH was generated (see SI 1 section and Supplementary Fig. S7d in Supporting Information). Based on these titration results, we can conclude that at this cosurfactant mole fraction [$X_{GOE} = 0.5$, $X_{OcA} = 0.5$], vesicles form at acidic pHs <5 and at extremely alkaline conditions (pH >10). Accordingly, GOE/OcA 1:1 mole ratio forms vesicles in the extreme range of pH conditions, similar to the decylamine/decanoic acid system (Namani and Deamer, 2008).

We also examined the phase behavior of a GOE/OcA 3:1 mole ratio [$X_{GOE} = 0.75$, $X_{OcA} = 0.25$] across a wide pH range (Figs. 2 and 3). The base titration experiment indicated that vesicles formed between pH $\sim$4–7 and oil droplets formed at pH >7 (Figs. 2a, d and 3b). Thus, the pH range for vesicle formation can be improved to a much wider range by simply adjusting the mole ratio of GOE/OcA from 1:1 to 3:1.

We also examined the self-assembly behavior of GOE and OcOH at 1:1 and 3:1 mole ratios. These GOE/OcOH systems produce vesicles from pH 3 to 7, as confirmed by light microscopy, and no vesicles were observed at pH >7 (Supplementary Figs. S8 and S9). We also conducted a titration experiment for GOE/decanol (1:1) mole ratio, which showed similar behavior to the corresponding GOE/OcOH (1:1) system, which showed stable vesicles at pH $\sim$2–5 (data not shown).

3.3. Continuous variation

We used the CV principle to explore the self-assembly behavior of mixed GOE/OcA or GOE/OcOH systems over a wide range of mole fractions at pH $\sim$3–4 to determine the chemical compositions at which vesicles are formed. The pure GOE.HCl system appeared as a clear solution (pH $\sim$3–4), suggesting the presence of micelles (Fig. 4a, b). From an OcA mole fraction of $X_{OcA} = 0.1$ to $X_{OcA} = 0.5$, the solution became turbid, and the presence of vesicles was confirmed by light microscopy (Figs. 4a, b and 5a).

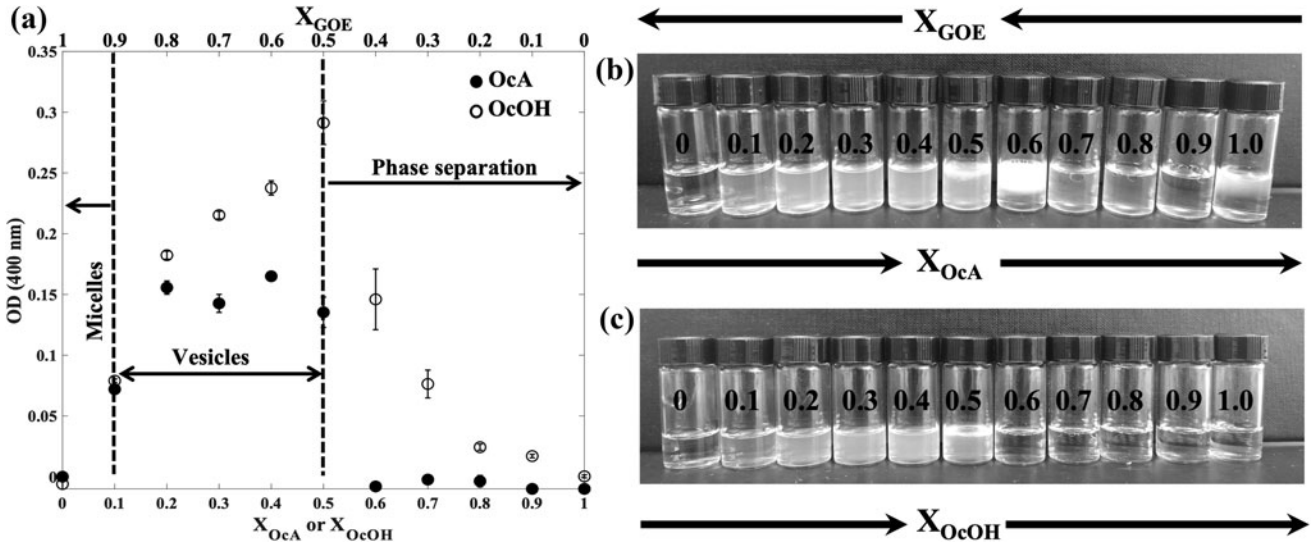

FIG. 4. Self-assembly behavior of mixed GOE/cosurfactant (OcA or OcOH) systems as a function of cosurfactant mole fraction at a total lipid concentration of 0.1 *M* (GOE+OcA or GOE+OcOH). **(a)** CV plots of optical density at 400 nm versus mole fraction of GOE (X_{GOE}) and OcA or OcOH (X_{OcA} or X_{OcOH}). The region of vesicle formation ($0.1 < X_{Cosurfactant} < 0.5$) is represented within the two vertical dashed lines. Error bars represent the standard deviation from the mean of three replicates. **(b, c)** The corresponding vial samples of GOE and OcA **(b)** or GOE and OcOH **(c)**, where the numbers on the vials represent the value of X_{OcA} or X_{OcOH}, respectively. CV = continuous variation.

At a value of $X_{OcA} > 0.5$, the suspension separated into an oil phase (Fig. 4b). These phase behaviors over the range of mole fractions were also consistent with the MD simulation results (see Section 3.5). Similar results were observed for the experimental GOE/OcOH system (Figs. 4c and 5b).

3.4. Effects of divalent ions and seawater

In addition to examining the pH range of GOE-based vesicle stability, we were also interested in the stability of these vesicles in the presence of divalent cations, because high concentrations of $\sim$0.075–0.08 *M* of Mg^{2+} or Fe^{2+} are required for RNA template-mediated RNA polymerization reactions (Jin *et al.*, 2018). Stable vesicles were observed for the GOE/OcA (1:1) mole ratio system by epifluorescence microscopy in the presence of high divalent cation concentration (0.1 *M* $MgCl_2$, pH 4) (Fig. 6a).

Separately, we examined pure OcA vesicles at pH 7.0 and pure OcA vesicles in the presence of 0.1 *M* $MgCl_2$, pH 4. Epifluorescence microscopy confirmed that pure OcA at pH 7.0 forms vesicles, but an oil phase is formed in the presence of 0.1 *M* $MgCl_2$ at pH 4 (Supplementary Fig. S10a, b). Thus,

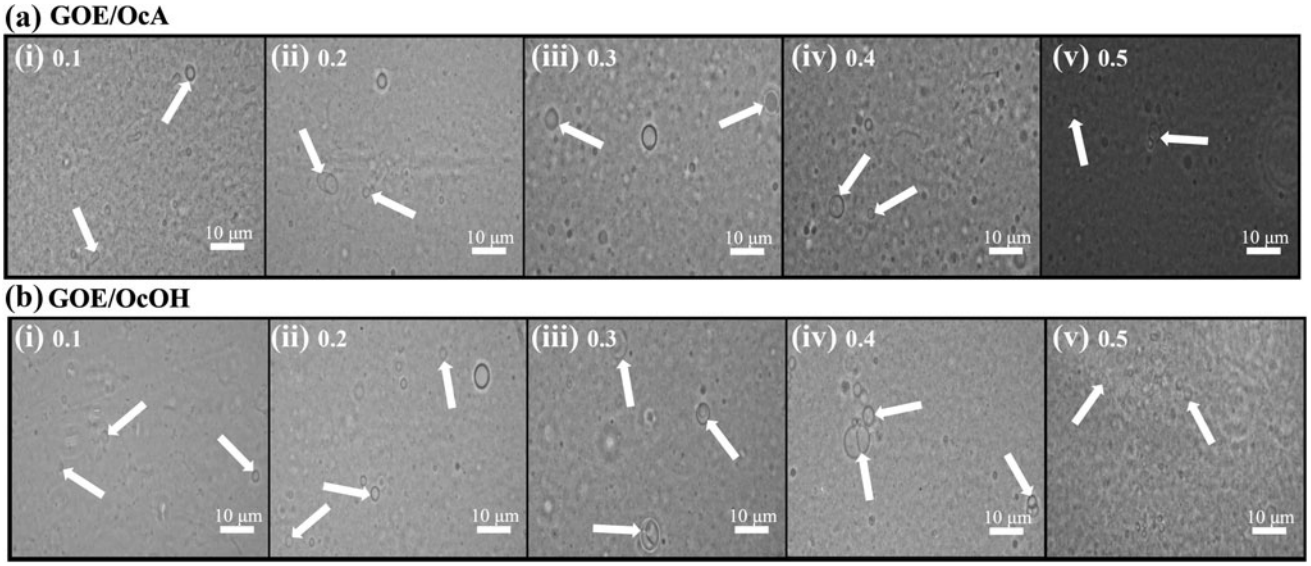

FIG. 5. Photomicrographs of GOE/cosurfactant OcA or OcOH CV mixture samples. **(a)** GOE/OcA CV samples, where the numbers on each panel correspond to Figure 4b and represent the value of X_{OcA}; **(b)** GOE/OcOH CV samples, where the numbers on each panel correspond to Figure 4c and represent the value of X_{OcOH}. Solid white arrows indicate vesicles. Total lipid concentration = 0.1 *M*.

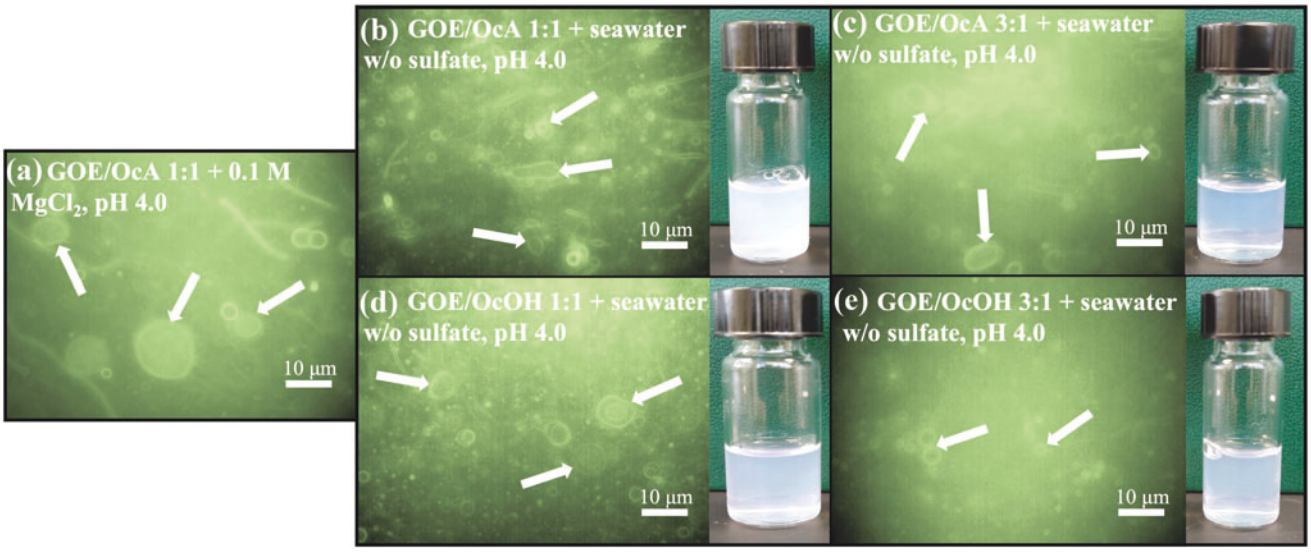

FIG. 6. Effect of divalent cations **(a)** and simulated Hadean seawater without sulfate **(b–e)** on GOE/cosurfactant systems. Perylene, a lipophilic dye molecule, was used (0.025 mol %) for visualization of the vesicle structures, which are indicated by sold white arrows. Total lipid concentration = 0.1 *M*. **(a)** GOE/OcA (1:1) mole ratio in the presence of 0.1 *M* $MgCl_2$ at pH 4; **(b)** GOE/OcA (1:1) and its corresponding vial at pH 4; **(c)** GOE/OcA (3:1) and its corresponding vial at pH 4; **(d)** GOE/OcOH (1:1) and its corresponding vial at pH 4; and **(e)** GOE/OcOH (3:1) and its corresponding vial at pH 4.

it is, indeed, the inclusion of GOE with OcA, which leads to vesicles being resistant to Mg^{2+}.

To test the stability of GOE-based vesicles in modern sea water, we prepared GOE/OcA or GOE/OcOH mixtures at 1:1 and 3:1 mole ratios. No vesicles were observed in these GOE/cosurfactant systems in simulated modern sea water (Supplementary Fig. S10c, d). We hypothesized that the flocculation of the surfactants was caused by the presence of SO_4^{2-} in the simulated seawater, but to confirm this, we systematically assessed the stability of each major ion present in the simulated sea water mixture separately. We found that Na_2SO_4 was responsible for the flocculation of GOE/cosurfactant vesicles; accordingly, we prepared sea water without the Na_2SO_4 component. Both GOE/OcA and GOE/OcOH (1:1) and (3:1) mixtures formed stable vesicles in this modified simulated seawater (Fig. 6b–e).

3.5. MD simulation systems

Dispersions of fatty acids in aqueous medium self-assemble into various structures, such as micelles, vesicles, and oil droplets, depending on the fatty acid identity and the dispersion method (Fameau *et al.*, 2014). In all of our simulated systems (single amphiphile molecule in vacuum or in implicit solvation, and multiple molecules with explicit solvation), a_s and l_c are directly measured from the simulations; alternatively, l_c is also estimated based on empirical Equation 2; and a constant value of v_c is estimated as defined in equation. The various GOE/OcA cosurfactant systems studied by MD simulations are summarized in Supplementary Table S2, and representative video segments of the production runs are provided in SI 4–8 with the corresponding video filenames reported in Supplementary Table S3.

The values of a_s and l_c obtained from the simulations and the corresponding calculated cpp values at pH ~3–4 for the various GOE/OcA mixtures are reported for the system with multiple amphiphile molecules in explicit solvation, and for the systems of individual molecules in vacuum or with implicit solvation, respectively (Table 1 and Supplementary Tables S4–S6). At low values of $X_{OcA} = 0$–0.04 where GOE is the dominant component, cpp values ranged between

Table 1. Calculated Critical Packing Parameter Values for Glycine *N*-Octyl Ester/Octanoic Acid Cosurfactant Systems at Various Mole Fractions of Octanoic Acid (X_{OcA}) and Glycine *N*-Octyl Ester (X_{GOE}) in Explicitly Solvated Molecular Dynamic Simulation Systems Modeling pH 4 Conditions

X_{GOE}	X_{OcA}	*Calculated cpp*	*Predicted structures*	*Experimentally observed structures*
1.0	0.0	0.583	Micelle/vesicle	Micelle
0.9	0.1	0.629	Vesicle	Vesicle
0.5	0.5	0.913	Vesicle	Vesicle
0.1	0.9	1.608	Oil (inverted micelle)	Oil
0.0	1.0	1.994	Oil (inverted micelle)	Oil

Predicted self-assembly behavior is compared with results from experimental observation. Values of l_c and a_s for each amphiphile were obtained for each system composition as average geometry weighted by the mole fraction of each component (see SI 3 section and Equations 1–3 in Supporting Information). Cpp-values <0.5 indicates micelles; cpp >1.0 indicates oil droplets/phase separation; and 0.5 < cpp <1.0 indicates vesicles.

cpp = critical packing parameter; GOE = glycine *n*-octyl ester; OcA = octanoic acid.

~0.58 and 0.9, predicting that vesicles should be stable (Table 1).

At equimolar concentrations of GOE and OcA, the calculated cpp value approached close to 1, which is still consistent with vesicles. As X_{OcA} increased toward 1 and (X_{GOE} decreased toward 0.0), the cpp values became >1, indicating oil formation at 100% GOE (Table 1). These results are broadly consistent with our experimental observations. Further, it is interesting to note that accounting for the effects of hydrophobic interactions by considering implicit solvation and explicit solvation only moderately altered the calculated cpp values compared with the corresponding vacuum values (Table 1 and Supplementary Tables S4–S6).

Alternative cpp values were also calculated using empirical l_c values (Equation 2). The empirical l_c values were about 29% greater and caused cpp values thus obtained to be ~22% lower than those obtained from the simulation geometry (data not shown).

Snapshots of representative amphiphile clusters in the explicitly solvated GOE/OcA system at $X_{GOE} = 1.0–0.0$ ($X_{OcA} = 0.0–1.0$) show that the size of the amphiphile clusters generally increases with increasing fatty acid content as the self-assembly behavior changes from micellar to vesicular to oil-like (left to right in Fig. 7a–e). Thus, qualitatively smaller sized self-assembled structures are seen in the pure GOE system compared with the self-assembly size in the mixed systems as OcA is added. The density maps also show that micellar structures tend to be smaller in size but greater in number and the trend reverses with increasing OcA content (left to right in Fig. 7f–j). These smaller GOE clusters at higher ratios of GOE/OcA are consistent with micellar type self-assembly observed in our experimental CV system (Fig. 4).

4. Discussion

4.1. Tentative GOE and IOE synthesis

Results from ESI-MS analysis reveal that both GOE and IOE were tentatively observed by subjecting a 1:1 mole ratio of amino acid and OcOH to wet-dry cycles at $T = 50°C$, but not at 80°C. In the glycine/OcOH spectrum at 80°C, a peak (*m/z* 137) corresponding to piperazine-2,5-dione, a cyclic dimer of glycine, was observed (Supplementary Fig. S1c and Supplementary Table S1). In addition, peaks corresponding to the deamination of glycine (*m/z* 83) and the reactant glycine plus a proton or sodium (*m/z* 76 or 98) were identified (Supplementary Fig. S1c and Supplementary Table S1).

We infer that GOE was not observed at 80°C potentially due to various factors, including hydrolysis of the GOE ester bond driven by a lower activation barrier at higher

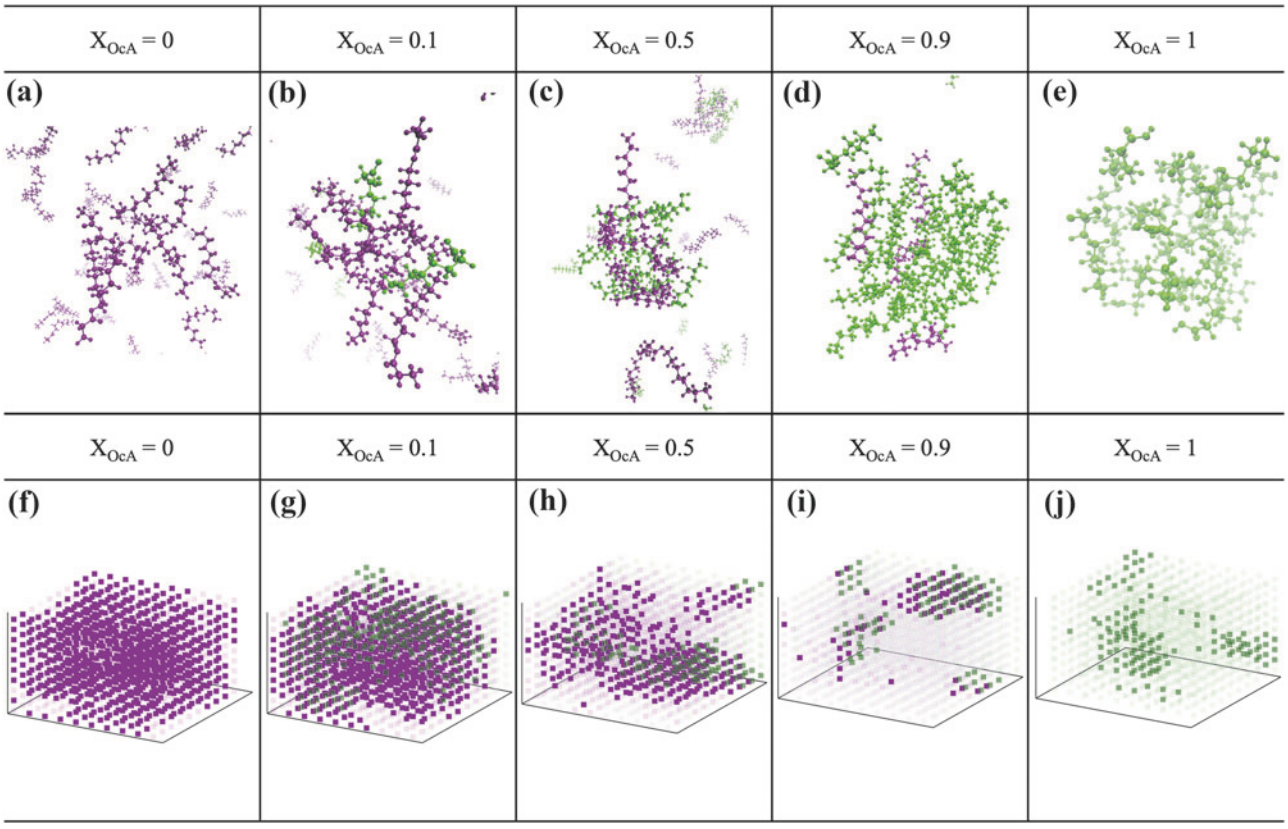

FIG. 7. Self-assembly in pure and mixed GOE/OcA systems at various OcA mole fractions ($X_{OcA} = 0.0–1.0$) obtained by molecular dynamics simulations in explicit solvent. The GOE molecules are shown in purple, and OcA molecules are shown in green. **(a–e)** snapshots of representative clusters of GOE and OcA; **(f–j)** density maps showing amphiphile distributions of GOE and OcA. The entire cubic simulation box is shown ($10 \times 10 \times 10\,nm^3$). Dim and bright portions correspond to low- and high-density patches, respectively. Water molecules and Cl^- ions are not shown for clarity.

temperature and/or the formation of cyclic piperazine-2,5-dione, which may have prevented glycine from forming an ester bond with OcOH (Orgel, 1989). Similarly, in the isoleucine-OcOH system spectrum at 80°C, there are peaks corresponding to the reactant isoleucine plus hydrogen or sodium (*m/z* 132 or 154), again suggesting possible hydrolysis of the ester bond at this temperature (Supplementary Fig. S1d).

Comparison of the ESI-MS^2 spectra in Supplementary Figures S4 and S5 shows that glycine plus octanol may yield not only GOE, but also other products, such as octylglycine (structure I), shown in Supplementary Fig. S4. In fact, the fragments in Supplementary Fig. S4 at *m/z* 192 (water loss), 164 (water+CO loss, or loss of formic acid), and 147 (loss of water+CO+NH_3) are consistent with structure (I), which could be the main product (Supplementary Fig. S4).

Although unlikely in the bulk solution, it is hypothesized that the microcompartment provided from either the reaction conditions or electrospray source may have increased the favorability of alkylation on the primary amine of glycine, producing a mixture of both octyl glycinate (GOE) and octylglycine. Several unfavorable condensation reactions have recently been reported as occurring nonenzymatically in microdroplets, micelles, thin films, and soft interfaces (Badu-Tawiah *et al.*, 2012; Fallah-Araghi *et al.*, 2014; Lee *et al.*, 2015; Nam *et al.*, 2017; Lee *et al.*, 2019; Ansu-Gyeabourh *et al.*, 2020), and the underlying mechanisms are still being investigated (Rovelli *et al.*, 2020; Xiong *et al.*, 2020). Microcompartments in geochemical and atmospheric systems are widely abundant, so the formation of octylglycine stabilized by its complementary cationic isomer, GOE, could potentially offer a one-step synthesis to a cosurfactant mixture (Supplementary Fig. S4c-I, II).

However, it is necessary to address inconsistencies in synthesis products observed in Supplementary Figures S1 and S4. As seen in Supplementary Figure S1, only the putative protonated ion of GOE (*m/z* 188) was observed, whereas both the protonated ion and the sodiated ion (*m/z* 210) were observed in Supplementary Figure S4. This indicates that the sodiated ion, which was isolated for ESI-MS^2 due to an inability to exclude the glycine trimer (*m/z* 189) from the ion trap (Supplementary Fig. S4), does not appear consistently in our synthesis experiments. This inconsistency, in combination with the observation of other products—such as octylglycine—in our synthesis products, suggests that GOE is not easily formed from glycine and OcOH under the current conditions used. As a result, we have labeled this a *tentative* synthesis, and we are presently investigating the esterification reaction under other conditions.

Based on the earlier cited results, it appears that a balance of factors must be maintained for the tentative synthesis of amino acid-fatty alcohol ester amphiphiles by wet-dry cycles. Such factors include a temperature high enough to drive the thermodynamics of condensation reactions in aqueous solution, but low enough to avoid breaching the activation barrier for ester hydrolysis. Further, the temperature should also be low enough to prevent the formation of other compounds that can inhibit ester bond formation.

In our systems, that balance was found at 50°C. Notably, our results demonstrate that both types of amino acid-fatty alcohol ester amphiphiles (GOE and IOE) can be tentatively synthesized under chemically simple, prebiotically plausible, and geologically realistic near-equilibrium conditions, thus increasing the likelihood that such amphiphiles may have comprised some of the most primitive protocell membranes. However, it must be noted again that this reaction, in its current form, does not consistently produce both the protonated and sodiated ions of GOE, and we have not investigated the effect that octylglycine, a GOE isomer, may have on vesicle stability.

4.2. GOE- and GOE/cosurfactant-based vesicles

A significant goal of this study was to examine the self-assembly behaviors of the novel, prebiotically plausible class of molecular chimera, amino acid-fatty alcohol esters. We examined a specific representative of this class of compounds, namely, GOE—both in its pure form and in mixtures with cosurfactants, OcA or OcOH or decanol (Fig. 1a). Results are summarized in Figure 8. The first set of titration experiments showed that GOE can, indeed, form vesicles by itself at a narrow pH range (7.3–8.2) (Fig. 2b).

When mixed with either OcA or OcOH, GOE/cosurfactant-based vesicles exhibit unprecedented stability across both a wide pH range and in the presence of divalent cations (Figs. 6 and 8). A GOE/OcA (1:1) mole ratio mixture forms vesicles that are stable at pH >10, and both GOE/OcA and GOE/OcOH at 1:1 mole ratio form stable vesicles at pH <4.5 (Figs. 2 and 8).

The stability range for vesicles can be further extended up from pH <3 to pH $\sim$7.5 by increasing the GOE/OcA or GOE/OcOH mole ratio to 3:1 [$X_{GOE} = 0.75$, $X_{Cosurfactant} = 0.25$] (Figs. 2 and 8). The GOE/cosurfactant (1:1) mole ratio systems are also stable in the presence of divalent cations and, significantly, the GOE/cosurfactant-based (1:1 and 3:1) vesicles are stable in simulated Hadean seawater that lacks SO_4^{2-} (Figs. 6 and 8).

Results from the CV experiment, combined with those of microscopy, calculated cpp values, and cluster densities, as well as self-assembled structure sizes from MD simulations, reveal that vesicles formed in the compositional range of $X_{GOE} = 0.5$–0.9 with OcA or OcOH making up the remainder of the mixture (Figs. 4, 5, and 8). These results demonstrate that only a small amount of cosurfactant ($X_{Cosurfactant} = 0.1$) is sufficient to form vesicles with GOE. Not only that, but there are also essentially no differences in the behavior of GOE/OcA and GOE/OcOH systems, with the exception of the GOE/OcA (1:1) system being additionally stable at pH >10 (Figs. 4 and 8).

By not differentiating between OcA or OcOH, the prebiotic plausibility of these GOE/cosurfactant vesicles is further extended to encompass a wider range of chemical inventories and geologic settings in early Earth where either of these cosurfactants could have been present.

4.3. Computational observations of GOE/cosurfactant self-assembly behavior

The predicted self-assembly behavior of the GOE/OcA system over the entire composition range based on all-atom MD simulations in the current work provided much useful insights to complement and help rationalize our experimental

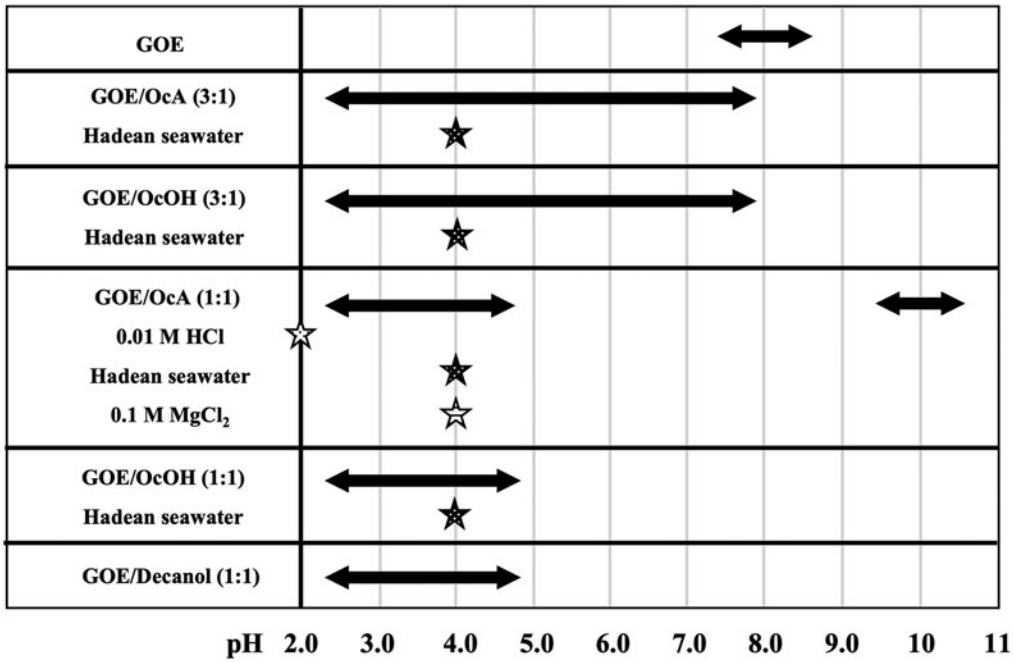

FIG. 8. Summary of the vesicle stability range of GOE/cosurfactant (OcA, OcOH, or decanol) systems at various mole ratios over a wide pH range and in the presence of ions and simulated Hadean seawater (without sulfate). The pH ranges for vesicle formation are indicated by the double-headed arrows. Stars are used to depict vesicle stability in 0.01 *M* HCl suspension, pH 2 (hollow star), 0.1 *M* $MgCl_2$ (striped star), and Hadean seawater (solid star) conditions.

results. The calculated cpp values were largely in agreement with our experimental results, evidencing the utility of simulations in predicting, at least to a first approximation, the self-assembly behavior of mixed amphiphile systems.

The cpp values obtained for the explicit solvation, vacuum, and implicit solvation systems were quite comparable (Supplementary Tables S4–S6). This suggests that, at the current all-atom resolution and at the current 0.025 μs simulation time spans, molecular shapes dictated by well-benchmarked intramolecular potential functions and inter-lipid interactions take precedence over solvophobic effects in driving the observed self-assembly behaviors.

The advantage of an all-atom simulation scheme as used in the current study lies in collecting accurate molecular shape information and calculation of cpp values. This allowed the prediction of the self-assembly behaviors on the nano second time scales, well before the onset of visually discernable self-assembled structures, that correspond to the experimental micellar, vesicular, or oil-like phases. Achieving these structures from random dispersions would require simulations on the order of microseconds, preferentially with coarse graining rather than at an all-atom resolution, so as to mitigate the large computational cost that would otherwise accrue. One previous study, for example, assessed large-scale self-assembled structures that arose from 4 μs simulations of differently ionized oleic acid molecules in water by employing a Martini force field-based coarse-grained model (Janke *et al.,* 2014).

An example of further refinement to the current calculations would be a precise calculation of the hydrophobic tail volume, v_c, that would give comparable statistical distribution as those obtained for l_c and a_s. In addition, the grid-based volumetric density maps obtained here may be further harnessed to exclude nonself-assembled molecules from the cpp calculations. Such a grid-based density map can help operationalize an atomic-density based delineation of cluster peripheries, which will, in turn, help quantify the number and size of self-assembled structures in each system.

4.4 Prebiotic relevance

Prebiotically plausible amphiphiles capable of forming early membranous compartments must exhibit at least the following characteristics: (i) be produced under prebiotic settings; (ii) be able to withstand harsh geological conditions; and (iii) have sufficient permeability to allow nutrients and waste to pass through the membrane. Fatty acids are considered to be among the most likely amphiphiles that made up protocell membranes, as they are found in carbonaceous meteorites along with other organic material.

The solvent-extracted organics from meteorites form self-assembled structures that resemble cell membranes (Deamer, 1985; Deamer *et al.*, 2002). The majority of research on protocell membranes thus far has focused on forming model protocells from decanoic acid since it is found in meteorites, and from oleic acid, which makes less leaky membranes than decanoic acid. However, Shimoyama *et al.* (1989) discovered that OcA, and nonanoic acid, both of which have shorter chain lengths compared with decanoic acid, are more abundant in meteorites. The OcA-based primitive membranes are not commonly explored, however, mainly due to their higher critical vesicle concentrations and greater leakiness than longer chain fatty acids (Budin *et al*., 2014).

Further, building protocells from fatty acids has various drawbacks, the most notable of which are pH stability within a very narrow range of geochemical conditions, such as pH ~7.0–8.5 and low divalent cation tolerance, which have proven to be long-standing hurdles in the protocell research field. In detail, as ionic strength increases (~0.5 *M* NaCl) fatty acid vesicles completely flocculate (Maurer and Nguyen, 2016; Cohen *et al.*, 2022; Monnard *et al.*, 2002). They are also more prone to phase separation in the presence of divalent cations (Mg^{2+}, Ca^{2+}, Fe^{2+}) at concentrations as low as 0.005 *M* (Dalai and Sahai, 2018).

The narrow pH stability range of pure fatty acid vesicles is especially problematic because solution pHs on early Earth could have ranged from acidic, due to high partial pressures of CO_2 gas in the early atmosphere, to neutral and alkaline after weathering reactions and wetting-drying cycles of postweathering solutions (Sahai *et al.*, 2022). Moreover, Mg^{2+} concentrations in these solutions would have ranged from millimolar in weathering solutions to sub-micromolar in evaporative brines (Sahai *et al.*, 2022).

Thus, primitive membranes existing in such conditions would have had to be stable across such a wide range of pH, salt, and temperature conditions (Dalai and Sahai, 2018). The chemical structure of a prebiotically plausible amphiphile capable of robust self-assembly into vesicles under a wide range of prebiotic geochemical conditions has neither been proposed nor synthesized previously.

In the present study, we hypothesized, and subsequently demonstrated, that amino acid-fatty alcohol ester amphiphiles, a molecular chimera that incorporates features of both amino acid and amphiphile fatty alkyl chains, meet the criteria required for robust protocell-membrane-forming amphiphiles. To the best of our knowledge, such a molecular chimera has never before been proposed, synthesized, and explored for self-assembly behavior.

The proof-of-concept was demonstrated here by the tentative synthesis of GOE and IOE with a small number of wet-dry cycles at moderate temperatures (50°C). Further, we hypothesized that such ester amphiphiles would be stable under a wide range of pH and salt conditions. Our results demonstrate that GOE/cosurfactant vesicles are stable in a wide pH range of 3–11. Notably, our results reveal an *adaptive* system whereby just changing the mole ratios—specifically from pure GOE to 1:1 [$X_{GOE} = 0.5$, $X_{Cosurfactant} = 0.5$] to 3:1 [$X_{GOE} = 0.75$, $X_{Cosurfactant} = 0.25$]—the pH range for vesicle stability can be extended to encompass pH 3–11, a range markedly wider than that of traditional fatty acid/cosurfactant (fatty amine or fatty alcohol) systems (Fig. 8).

Further, OcA, OcOH, and decanol behaved similarly in mixed GOE systems. Thus, the prebiotic plausibility of these GOE/cosurfactant vesicles is further extended to encompass a vast range of chemical inventories and geologic settings where either family of cosurfactant (fatty acid or fatty alcohol) may have been present on early Earth.

Even more impressive is the observation that GOE/cosurfactant systems are stable in the presence of divalent cations even at extremely low pHs (Fig. 6). The results of the modern seawater experiment revealed that Na_2SO_4 causes flocculation of GOE and GOE/cosurfactant vesicles, presumably due to charge-screening effects of SO_4^{2-} anion on the ammonium moiety of the GOE head group (Supplementary Fig. S10c, d). However, simulated Hadean seawater without SO_4^{2-} does not destabilize the vesicles (Fig. 6).

The Hadean Ocean likely had very low SO_4^{2-} concentrations of ~200 μ*M* due to the presence of an anoxic atmosphere and disproportionation of volcanogenic SO_2 into HS^- and SO_4^{2-} in aqueous solution (Holland, 2004; Sahai *et al.*, 2022). Thus, the novel chimeric amino acid-fatty alcohol ester amphiphile-based protocell membrane proposed here would have been stable over a wide range of geochemical environments. Beyond vesicle stability, our model system is an elegant demonstration of the concept of mutualism and synergism in the coevolution of biomolecules or their precursors in the origins of life (Kaddour and Sahai, 2014).

In a recent work, the Rajamani group reported using modern membrane-forming phospholipid hydrolysis in association with glycine to build primitive membrane compartments during wet-dry cycling at a temperature of 90°C (Joshi *et al.*, 2021). Those authors also demonstrated the synthesis of polyglycine. This is another excellent example of how biomolecules may work together to generate complex functional biopolymers, and this sentiment is reflected in our current work with GOE and IOE.

5. Conclusions

A large body of previous work on primitive membranes has focused on traditional fatty acid systems with fatty alcohols, fatty amines, fatty glycerol esters, and other cosurfactants to enhance the stability of vesicles over a wider range of pH conditions and presence of divalent cations. However, the majority of these vesicles form only in moderately alkaline conditions (pH ~7–8.5). Vesicles created using alkyl amines as the cosurfactant do form in acidic conditions, but alkyl amines are not typically considered prebiotically realistic, and these amphiphiles form micelles at highly alkaline pHs > ~8.5.

Here, we showed that amino acids can work cooperatively with fatty acids to create a novel, chemically simple, and prebiotically plausible chimeric amino acid-fatty alcohol ester amphiphile, which can be tentatively synthesized under relatively simple, prebiotically relevant near-equilibrium conditions. These amino acid-fatty alcohol ester amphiphiles, when mixed with cosurfactants, form stable model protocell membranes across a pH range of 3–11 and can withstand the presence of divalent cations at low pHs and the presence of simulated Hadean seawater.

This cooperation between biomolecules provides further evidence for the mutualistic coevolution—as opposed to sequential development—of biomolecules or their precursors. This proof-of-concept study is currently being expanded to include other amino acids and fatty alcohol esters as part of an effort in cataloging a robust class of protocell membrane-forming prebiotic amphiphiles, which could have ensured protocell survival in a wide range of geochemical settings.

Acknowledgments

The authors are also grateful to Dr. Saúl Villafañe-Barajas for his artistic contributions toward the graphical abstract, to Hannah Durr for her assistance with some microscopy images, and to Addie Keating at the University of Akron Mass Spectrometry Center for her assistance with ESI-MS and ESI-MS^2.

Author Disclosure Statement

The authors declare that a few days before submitting this manuscript, they were kindly informed by Dr. Sarah Maurer, Central Connecticut State University, that her research group has been working independently on a similar project involving amino acid-fatty alcohol amphiphiles, and that she has recently become aware of their work through our abstract at the Astrobiology Science Conference 2022. We mutually and respectfully agreed to acknowledge the independent intellectual contributions of the two teams and to make this declaration in both their group publications on this research topic.

Funding Information

Financial support was provided to Nita Sahai by NSF EAR award number 1829695 and NASA 80NSSC18K1139 subaward RK558-G2. Generous private gift funds from Dr. Ed Weil to Nita Sahai are also gratefully acknowledged. Chrys Wesdemiotis is funded by grant award number CHE-1808115.

Supplementary Material

Supplementary Information
Supplementary Table S1
Supplementary Table S2
Supplementary Table S3
Supplementary Table S4
Supplementary Table S5
Supplementary Table S6
Supplementary Figure S1
Supplementary Figure S2
Supplementary Figure S3
Supplementary Figure S4
Supplementary Figure S5
Supplementary Figure S6
Supplementary Figure S7
Supplementary Figure S8
Supplementary Figure S9
Supplementary Figure S10

References

Ansu-Gyeabourh E, Amoah E, Ganesa C, *et al*. Monoacylation of symmetrical diamines in charge microdroplets. *J Am Soc Mass Spectrom* 2020;32(2):531–536.

Apel CL, Deamer DW. The formation of glycerol monodecanoate by a dehydration condensation reaction: Increasing the chemical complexity of amphiphiles on the early earth. *Orig Life Evol Biosph* 2005;35(4):323–332; doi: 10.1007/s11084-005-2046-8

Apel CL, Deamer DW, Mautner MN. Self-assembled vesicles of monocarboxylic acids and alcohols: Conditions for stability and for the encapsulation of biopolymers. *Biochim Biophys Acta* 2002;1559(1):1–9; doi: 10.1016/s0005-2736(01)00400-x

Badu-Tawiah AK, Campbell DI, Cooks RG. Accelerated C–N bond formation in dropcast thin films on ambient surfaces. *J Am Soc Mass Spectrom* 2012;23(9):1461–1468.

Bekker H, Berendsen H, Dijkstra E, *et al.* Gromacs—A Parallel Computer for Molecular-Dynamics Simulations. In: *4th International Conference on Computational Physics (PC 92)* (DeGroot RA, Nadrchal J. Eds.). World Scientific Publishing: Singapore; 1993; pp. 252–256.

Beltrán-Gracia E, López-Camacho A, Higuera-Ciapara I, *et al*. Nanomedicine review: Clinical developments in liposomal applications. *Cancer Nanotechnol* 2019;10(1):11; doi: 10.1186/s12645-019-0055-y

Berclaz N, Müller M, Walde P, *et al.* Growth and transformation of vesicles studied by ferritin labeling and cryotransmission electron microscopy. *J Phys Chem B* 2001; 105(5):1056–1064; doi: 10.1021/jp001298i

Berendsen HJ, van der Spoel D, van Drunen R. GROMACS: A message-passing parallel molecular dynamics implementation. *Comput Phys Commun* 1995;91(1–3):43–56.

Black RA, Blosser MC, Stottrup BL, *et al*. Nucleobases bind to and stabilize aggregates of a prebiotic amphiphile, providing a viable mechanism for the emergence of protocells. *Proc Natl Acad Sci U S A* 2013;110(33):13272–13276; doi: 10.1073/pnas.1300963110

Bonfio C, Caumes C, Duffy CD, *et al.* Length-selective synthesis of acylglycerol-phosphates through energy-dissipative cycling. *J Am Chem Soc* 2019;141(9):3934–3939; doi: 10.1021/jacs.8b12331

Bonfio C, Russell DA, Green NJ, *et al*. Activation chemistry drives the emergence of functionalised protocells. *Chem Sci* 2020;11(39):10688–10697.

Budin I, Prywes N, Zhang N, *et al.* Chain-length heterogeneity allows for the assembly of fatty acid vesicles in dilute solutions. *Biophys J* 2014;107(7):1582–1590; doi: 10.1016/j.bpj.2014.07.067

Cantor CR, Schimmel PR. *Biophysical Chemistry Part III: The Behavior of Biological Macromolecules.* W. H Freeman and Co.: Oxford; 1980.

Chen IA, Szostak JW. A kinetic study of the growth of fatty acid vesicles. *Biophys J* 2004;87(2):988–998; doi: 10.1529/biophysj.104.039875

Chen IA, Roberts RW, Szostak JW. The emergence of competition between model protocells. *Science* 2004;305(5689):1474–1476; doi: 10.1126/science.1100757

Chen IA, Salehi-Ashtiani K, Szostak JW. RNA catalysis in model protocell vesicles. *J Am Chem Soc* 2005;127(38):13213–13219.

Cistola DP, Hamilton JA, Jackson D, *et al*. Ionization and phase behavior of fatty acids in water: Application of the Gibbs phase rule. *Biochemistry* 1988;27(6):1881–1888.

Cohen ZR, Cornell CE, Catling DC, *et al*. Prebiotic protocell membranes retain encapsulated contents during flocculation, and phospholipids preserve encapsulation during dehydration. *Langmuir* 2022;38(3):1304–1310; doi: 10.1021/acs.langmuir.1c03296

Cornell CE, Black RA, Xue M, *et al.* Prebiotic amino acids bind to and stabilize prebiotic fatty acid membranes. *Proc Natl Acad Sci U S A* 2019;116(35):17239–17244; doi: 10.1073/pnas.1900275116

Dalai P, Sahai N. Protocell Emergence and Evolution. In: *Handbook of Astrobiology* (Kolb VM. Ed.). CRC Press: Boca Raton, FL; 2018; pp. 491–520.

Dalai P, Sahai N. Mineral–lipid interactions in the origins of life. *Trends Biochem Sci* 2019a;44(4):331–341.

Dalai P, Sahai N. A model protometabolic pathway across protocell membranes assisted by photocatalytic minerals. *J Phys Chem C* 2019b;124(2):1469–1477.

Dalai P, Kaddour H, Sahai N. Incubating life: Prebiotic sources of organics for the origin of life. *Elements* 2016;12(6):401–406.

Dalai P, Ustriyana P, Sahai N. Aqueous magnesium as an environmental selection pressure in the evolution of phospho-

lipid membranes on early earth. *Geochim Cosmochim Acta* 2018;223:216–228.

Darden T, York D, Pedersen L. Particle mesh Ewald: An N·log (N) method for Ewald sums in large systems. *J Chem Phys* 1993;98(12):10089–10092.

Deamer DW. Boundary structures are formed by organic components of the Murchison carbonaceous chondrite. Nature 1985;317(6040):792–794; doi: 10.1038/317792a0

Deamer DW, Dworkin JP. Chemistry and Physics of Primitive Membranes. In: *Prebiotic Chemistry, Topics in Current Chemistry* (Walde P. Ed.). Springer-Verlag; 2005; pp. 1–27; doi: 10.1007/b136806

Deamer D, Dworkin JP, Sandford SA, *et al*. The first cell membranes. *Astrobiology* 2002;2(4):371–381.

Fallah-Araghi A, Meguellati K, Baret J-C, *et al*. Enhanced chemical synthesis at soft interfaces: A universal reaction-adsorption mechanism in microcompartments. *Phys Rev Lett* 2014;112(2):028301.

Fameau A-L, Arnould A, Saint-Jalmes A. Responsive self-assemblies based on fatty acids. *Curr Opin Coll Interf Sci* 2014;19(5):471–479.

Frenkel-Pinter M, Haynes JW, Mohyeldin AM, *et al.* Mutually stabilizing interactions between proto-peptides and RNA. *Nat Commun* 2020;11(1):1–14.

Hanczyc MM, Fujikawa SM, Szostak JW. Experimental models of primitive cellular compartments: Encapsulation, growth, and division. *Science* 2003;302(5645):618–622; doi: 10.1126/science.1089904

Hanwell MD, Curtis DE, Lonie DC, *et al*. Avogadro: An advanced semantic chemical editor, visualization, and analysis platform. *J Cheminform* 2012;4(1):1–17.

Harayama T, Riezman H. Understanding the diversity of membrane lipid composition. *Nat Rev Mol Cell Biol* 2018; 19(5):281–296; doi: 10.1038/nrm.2017.138

Hargreaves WR, Mulvihill S, Deamer D. Synthesis of phospholipids and membranes in prebiotic conditions. *Nature* 1977;266(5597):78–80.

Holland H. The geologic history of seawater. *Treat Geochem* 2004;6:583–625.

Israelachvili JN, Mitchell DJ, Ninham BW. Theory of self-assembly of lipid bilayers and vesicles. *Biochim Biophys Acta* 1977;470(2):185–201.

Janke JJ, Bennett WD, Tieleman DP. Oleic acid phase behavior from molecular dynamics simulations. *Langmuir* 2014; 30(35):10661–10667.

Jin L, Engelhart AE, Zhang W, *et al*. Catalysis of template-directed nonenzymatic RNA copying by Iron (II). *J Am Chem Soc* 2018;140(44):15016–15021.

Jo S, Kim T, Iyer VG, *et al.* CHARMM-GUI: A web-based graphical user interface for CHARMM. *J Comput Chem* 2008;29(11):1859–1865.

Job P. Formation and stability of inorganic complexes in solution. *Ann Chim* 1928;9:113–203.

Jordan SF, Nee E, Lane N. Isoprenoids enhance the stability of fatty acid membranes at the emergence of life potentially leading to an early lipid divide. *Interface Focus* 2019a;9(6): 20190067; doi: 10.1098/rsfs.2019.0067

Jordan SF, Rammu H, Zheludev IN, *et al.* Promotion of protocell self-assembly from mixed amphiphiles at the origin of life. *Nat Ecol Evol* 2019b;3(12):1705–1714; doi: 10.1038/s41559-019-1015-y

Jorgensen WL, Chandrasekhar J, Madura JD, *et al*. Comparison of simple potential functions for simulating liquid water. *J Chem Phys* 1983;79(2):926–935.

Joshi MP, Sawant AA, Rajamani S. Spontaneous emergence of membrane-forming protoamphiphiles from a lipid–amino acid mixture under wet–dry cycles. *Chem Sci* 2021;12(8): 2970–2978; doi: 10.1039/d0sc05650b

Kaddour H, Sahai N. Synergism and mutualism in nonenzymatic RNA polymerization. *Life* 2014;4(4):598–620.

Kaddour H, Gerislioglu S, Dalai P, *et al*. Nonenzymatic RNA oligomerization at the mineral–water interface: An insight into the adsorption–polymerization relationship. *J Phys Chem C* 2018;122(51):29386–29397; doi: 10.1021/acs.jpcc.8b10288

Lee JK, Banerjee S, Nam HG*, et al*. Acceleration of reaction in charged microdroplets. *Q Rev Biophys* 2015;48(4):437–444.

Lee JK, Walker KL, Han HS, *et al.* Spontaneous generation of hydrogen peroxide from aqueous microdroplets. *Proc Natl Acad Sci U S A* 2019;116(39):19294–19298.

Luisi PL, Stano P, Mavelli F. A possible route to prebiotic vesicle reproduction. *Artificial Life* 2004;10(3):297–308.

MacKerell Jr. AD, Bashford D, Bellott M, *et al*. All-atom empirical potential for molecular modeling and dynamics studies of proteins. *J Phys Chem B* 1998;102(18):3586–3616.

Maheen G, Tian G, Wang Y, *et al.* Resolving the enigma of prebiotic C- O- P bond formation: Prebiotic hydrothermal synthesis of important biological phosphate esters. *Heteroat Chem* 2010;21(3):161–167.

Mansy SS. Membrane transport in primitive cells. *Cold Spring Harb Perspect Biol* 2010;2(8):a002188–a002188; doi: 10.1101/cshperspect.a002188

Maurer SE, Nguyen G. Prebiotic vesicle formation and the necessity of salts. *Orig Life Evol Biosph* 2016;46(2):215–222.

Maurer SE, Tølbøl Sørensen K, Iqbal Z, *et al.* Vesicle self-assembly of monoalkyl amphiphiles under the effects of high ionic strength, extreme pH, and high temperature environments. *Langmuir* 2018;34(50):15560–15568.

McLafferty FW. Mass spectrometric analysis. Molecular rearrangements. *Anal Chem* 1959;31(1):82–87.

Monnard P-A, Walde P. Current ideas about prebiological compartmentalization. *Life* 2015;5(2):1239–1263.

Monnard P-A, Apel CL, Kanavarioti A, *et al*. Influence of ionic inorganic solutes on self-assembly and polymerization processes related to early forms of life: Implications for a prebiotic aqueous medium. *Astrobiology* 2002;2(2):139–152.

Nam I, Lee JK, Nam HG, *et al*. Abiotic production of sugar phosphates and uridine ribonucleoside in aqueous microdroplets. *Proc Natl Acad Sci U S A* 2017;114(47):12396–12400.

Namani T, Deamer DW. Stability of model membranes in extreme environments. *Orig Life Evol Biosph* 2008;38(4):329–341.

Namani T, Walde P. From decanoate micelles to decanoic acid/dodecylbenzenesulfonate vesicles. *Langmuir* 2005;21(14): 6210–6219.

Namani T, Snyder S, Eagan JS, *et al.* Amino acid specific nonenzymatic montmorillonite-promoted RNA polymerization. *Chem Sys Chem* 2021;3(3):e2000060.

Orgel LE. The origin of polynucleotide-directed protein synthesis. *J Mol Evol* 1989;29(6):465–474.

Patel BH, Percivalle C, Ritson DJ, *et al.* Common origins of RNA, protein and lipid precursors in a cyanosulfidic protometabolism. *Nat Chem* 2015;7(4):301–307.

Ramanathan M, Shrestha LK, Mori T, *et al.* Amphiphile nanoarchitectonics: From basic physical chemistry to advanced applications. *Phys Chem Chem Phys* 2013;15(26):10580–10611.

Rao M, Eichberg J, Oró J. Synthesis of phosphatidylcholine under possible primitive Earth conditions. *J Mol Evol* 1982; 18(3):196–202.

Rao M, Eichberg J, Oró J. Synthesis of phosphatidylethanolamine under possible primitive earth conditions. *J Mol Evol* 1987;25(1):1–6.

Rovelli G, Jacobs MI, Willis MD*, et al*. A critical analysis of electrospray techniques for the determination of accelerated rates and mechanisms of chemical reactions in droplets. *Chem Sci* 2020;11(48):13026–13043.

Ruiz-Mirazo K, Briones C, de la Escosura A. Prebiotic systems chemistry: New perspectives for the origins of life. *Chem Rev* 2014;114(1):285–366.

Sahai N, Kaddour H, Dalai P. The transition from geochemistry to biogeochemistry. *Elements* 2016;12(6):389–394.

Sahai N, Kaddour H, Dalai P*, et al*. Mineral surface chemistry and nanoparticle-aggregation control membrane self-assembly. *Sci Rep* 2017;7(1):43418.

Sahai N, Adebayo S, Schoonen MA. Freshwater and evaporite brine compositions on Hadean Earth: Priming the origins of life *Astrobiology* 2022;22(6):641–671; doi: 10.1089/ast.2020.2396

Sarkar S, Dagar S, Verma A, *et al.* Compositional heterogeneity confers selective advantage to model protocellular membranes during the origins of cellular life. *Sci Rep* 2020;10(1): 4483.

Sephton MA. Organic compounds in carbonaceous meteorites. *Nat Prod Rep* 2002;19(3):292–311.

Shao Y, Gan Z, Epifanovsky E, *et al*. Advances in molecular quantum chemistry contained in the Q-Chem 4 program package. *Mol Phys* 2015;113(2):184–215.

Shimoyama A, Naraoka H, Komiya M, *et al*. Analyses of carboxylic acids and hydrocarbons in Antarctic carbonaceous chondrites, Yamato-74662 and Yamato-793321. *Geochem J* 1989;23(4):181–193; doi: 10.2343/geochemj.23.181

Simoneit BR, Rushdi AI, Deamer DW. Abiotic formation of acylglycerols under simulated hydrothermal conditions and self-assembly properties of such lipid products. *Adv Space Res* 2007;40(11):1649–1656.

Stano P. Question 7: New aspects of interactions among vesicles. *Orig Life Evol Biosph* 2007;37(4):439–444.

Szostak JW, Bartel DP, Luisi PL. Synthesizing life. *Nature* 2001;409(6818):387–390.

Toparlak ÖD, Karki M, Egas Ortuno V, *et al*. Cyclophospholipids increase protocellular stability to metal ions. *Small* 2020;16(27):1903381.

Xiong H, Lee JK, Zare RN, *et al.* Strong electric field observed at the interface of aqueous microdroplets. *J Phys Chem* Lett 2020;11(17):7423–7428.

Zhou X, Dalai P, Sahai N. Semipermeable mixed phospholipid-fatty acid membranes exhibit K^+/Na^+ selectivity in the absence of proteins. *Life* 2020;10(4):39.

Address correspondence to:
Trishool Namani
School of Polymer Science and Polymer Engineering
University of Akron
170 University Avenue
Akron, OH 44325
USA

E-mail: tnamani@uakron.edu

Nita Sahai
School of Polymer Science and Polymer Engineering
University of Akron
170 University Avenue
Akron, OH 44325
USA

E-mail: sahai@uakron.edu

Submitted 25 April 2022
Accepted 28 December 2022

Abbreviations Used

ACN = acetonitrile
CAD = collisionally activated dissociation
cpp = critical packing parameter
CV = continuous variation
DAPI = 4′,6-diamidino-2-phenylindole
ESI-MS^2 = tandem ESI-MS
ESI-MS = electrospray ionization–mass spectrometry
GOE = glycine *n*-octyl ester
GOE.HCl = glycine *n*-octyl ester hydrochloride
IOE = isoleucine *n*-octyl ester
MD = molecular dynamic
OcA = octanoic acid
OcOH = octanol